ACS APPLIED MATERIALS & INTERFACES

Research Article

www.acsami.org

A Switchable *bis*-Branched [1]Rotaxane featuring Dual-Mode Molecular Motions and Tunable Molecular Aggregation

Hong Li,[†] Xin Li,[‡] Zhan-Qi Cao,[†] Da-Hui Qu,*[,†] Hans Ågren,[‡] and He Tian[†]

[†]Key Laboratory for Advanced Materials and Institute of Fine Chemicals, East China University of Science & Technology, Shanghai 200237, People's Republic of China

[‡]Division of Theoretical Chemistry and Biology, School of Biotechnology, KTH Royal Institute of Technology, Stockholm SE-10691, Sweden

Supporting Information

ABSTRACT: A multifunctional *bis*-branched [1]rotaxane containing a perylene bisimide (PBI) core and two identical bistable[1]rotaxane arms terminated with ferrocene units was prepared and characterized by ^{1}H NMR, ^{13}C NMR, and 2D ROESY NMR spectroscopies and by HR-ESI spectrometry. The system is shown to possess several key features: (1) In acetone solution, external acid−base stimuli can result in relative mechanical movements of its ring and thread, which can induce extension and contraction movements of the whole system accompanied by a rotational movement of the ferrocene units, thus realizing dual-mode molecular motions, and the optimized conformations at different states are obtained through molecular dynamics simulations employing the general Amber force field. (2) The introduction of PBI enables the system fluorescence encoding through distance-dependent photoinduced electron transfer process from the ferrocene units to the PBI fluorophore. (3) The addition of Zn^{2+} can increase the degree of aggregation of the system, while adding base hinders aggregation because of the movement of the macrocycle. The tunable aggregated nanostructural morphologies of [1]rotaxane were examined by scanning electron microscopy. These results can pave the way to achieve precise control of integrated and coupling nanomechanical motions at a single-molecule level and provide more insight into controlling the aggregate behavior of switchable mechanically interlocked molecules.

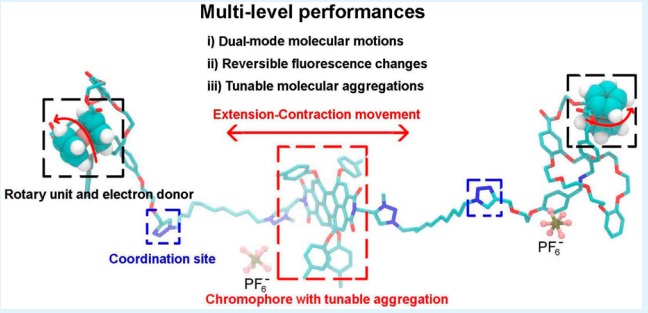

KEYWORDS: *bistable rotaxanes, perylene bisimide, fluorescence, dual-mode motions, tunable aggregation*

INTRODUCTION

Inspired by naturally occurring biological motors, such as the ATPase rotary motor and the kinesin or myosin linear motor systems,[1] chemists have constructed a variety of artificial molecular machines,[2−8] such as unidirectional rotors,[9,10] shuttles,[11−15] scissors,[16−18] and even molecular muscles,[19−22] elevators,[23−25] and walkers[26−30] that can perform diverse molecular motions. The control of molecular motion is the key in the design of a molecular machine system. However, the realization of controllable dual-mode motions in a single molecular system still remains a great challenge.[17] A bistable [1]rotaxane, in which a thread part is covalently connected with and threaded into a macrocycle, is an interesting species of the family of mechanically interlocked molecules (MIMs)[2−8] due to its rather unique and appealing architecture and tunable physical properties such as conductivity,[31] fluorescence,[32,33] electrochemical signals,[34] and circular dichroism.[35,36] In a bistable [1]rotaxane system, it is possible to realize controllable coupling of multiple mechanical motions by introducing a specific moving unit at the terminal of the molecular system. Controllable molecular aggregation with well-organized morphologies of organic functional molecules remains a hot topic because of their potential applications in the fields of molecular electronics and catalysis.[37,38] Introducing a specific chromophore perylene bisimide (PBI) into bistable rotaxanes can provide the possibility of alteration of molecular aggregation via the reversible moving of a macrocycle along a thread.[39] However, to the best of our knowledge, a mechanically interlocked system that can combine multilevel performances, such as dual-mode molecular motions and tunable molecular aggregations, still remains unexplored.

In this work, we report a new bistable *bis*-branched [1]rotaxane (Scheme 1) that can combine the performances of dual-mode molecular motions and tunable nanostructural morphologies in a single molecular system, which can provide more insight into the application of MIMs. As shown in Scheme 1, the multifunctional *bis*-branched [1]rotaxane Fc−PBI has two mechanically interlocked [1]rotaxane arms containing two distinguishable stations, namely, a dibenzylammonium (DBA)[40−42] and a *N*-methyltriazolium (MTA)[43−45]

Received: July 21, 2014
Accepted: October 10, 2014
Published: October 10, 2014

Scheme 1. (a) Chemical Structure of Target [1]Rotaxane and (b) Preparation of Target [1]Rotaxane and Conformations in Response to Chemical Stimuli

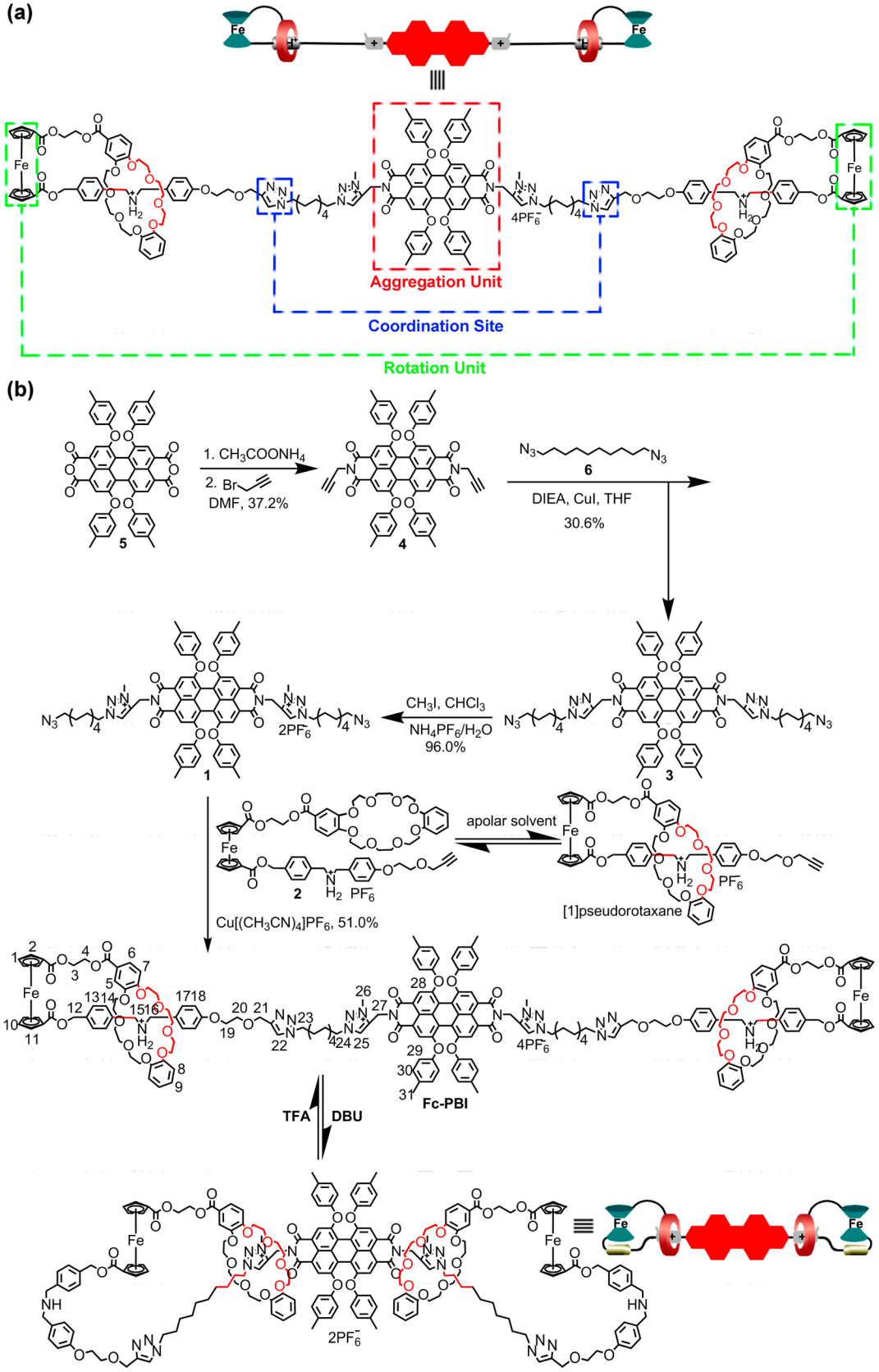

recognition station for dibenzo[24]crown-8 (DB24C8) ring and a terminal ferrocene[46−48] (Fc) unit situated at each end of the rotaxane arm that is introduced as a rotary moving part and an electron-donating functional unit. A PBI fluorescent dye was

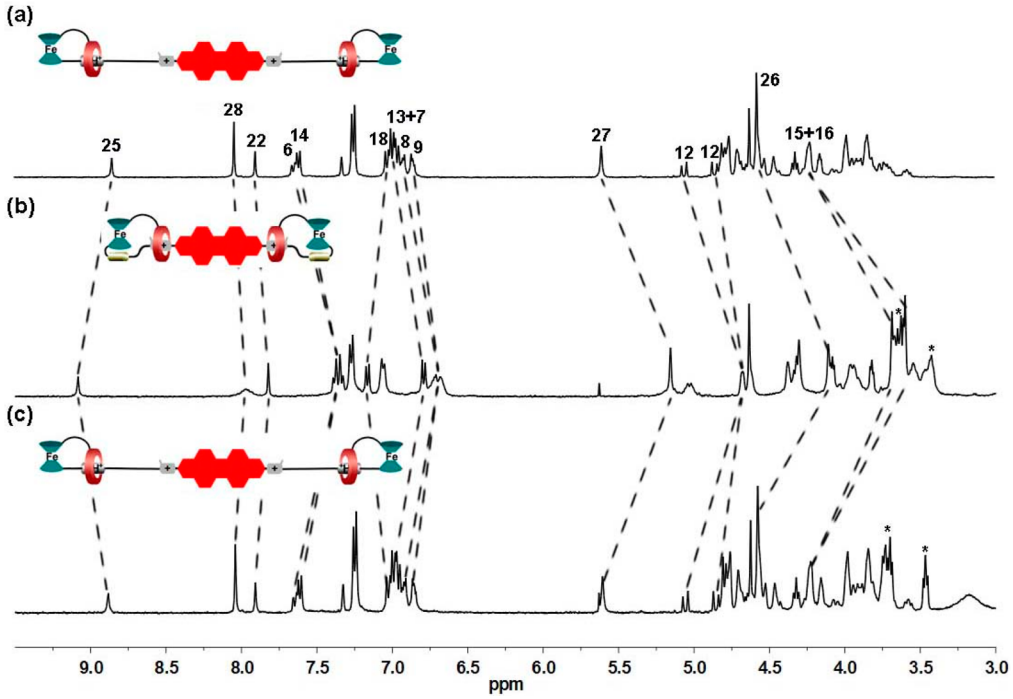

Figure 1. Partial ^{1}H NMR spectra (400 MHz, CD_3COCD_3, 298 K, 2.0×10^{-3} M) of (a) Fc−PBI, (b) deprotonation with addition of 2.5 equiv of DBU to sample a, and (c) reprotonation with addition of 5.0 equiv of TFA to sample b, where * denotes the residual proton signals of DBU.

introduced as a bridge to separate the two [1]rotaxane arms because of its remarkable photostability and controllable molecular aggregation properties.[49−55] A 1,2,3-triazole unit is located on the rotaxane thread to separate the two recognition sites, designed as a coordination site[56,57] with a transition metal to tune the aggregation degree of the PBI unit.

This *bis*-branched [1]rotaxane system is shown to undergo relative mechanical movements of its macrocyclic ring and thread in response to external acid−base stimuli and generated a remarkable fluorescence signal output visually. The time-evolution of the structures at the two states obtained from molecular dynamics (MD) simulations showed that the system can mimic the extension and contraction function of an artificial molecular muscle, and accompanied by simultaneous molecular rotation of the ferrocene unit, thus realizing the dual-mode coupling motions. Moreover, the introduction of a PBI unit into the center of the rotaxane can provide diverse nano-structural morphologies of the molecule under different external stimuli, indicating that the degree of the molecular aggregation can be altered by the chemically driven motion of the macrocycle or by the addition of transition metal Zn^{2+} to coordinate with the 1,2,3-triazoles of the rotaxane Fc−PBI. In particular, deprotonation of the DBA unit triggers the motion of the macrocycle to the MTA unit and decreases in the degree of aggregation, while the addition of Zn^{2+} ions results in enhancement in the degree of molecular aggregation. This study benefits us to better understand how to design multifunctional molecular machines with specific motion types and provides us with more insight of possible applications of switchable MIMs in the solid state.

RESULTS AND DISCUSSION

Syntheses. The target [1]rotaxane Fc−PBI is shown in Scheme 1. Starting from the derivative of 1,6,7,12-tetrachlor-operylene tetracarboxylic acid dianhydride **5**, imidization with ammonium acetate, then treatment with sodium hydride, and subsequent nucleophilic substitution with 3-bromopropyne, further copper(I)-catalyzed Huisgen 1,3-dipolar cycloaddition reaction with excess diazide compound **6** in the presence of CuI and *N*,*N*-diisopropylethylamine, followed by methylation with CH_3I and anion exchange with NH_4PF_6 aqueous solution could give azide **1** with a secondary MTA unit in a high yield (96%). As demonstrated in our previous studies,[33,34] compound **2** can form a predominantly self-complexing [1]pseudorotaxane structure in a polar solvent CH_2Cl_2, and subsequently, the well-known "click" reaction with azide **1** can produce the target [1]rotaxane Fc−PBI in a moderate yield (51%). The key intermediates and the target [1]rotaxane Fc−PBI were characterized by ^{1}H NMR and ^{13}C NMR spectroscopies and high-resolution electrospray ionization (HR-ESI) mass spectrometry. The HR-ESI mass spectrum of [1]rotaxane Fc−PBI features the most intense peaks at m/z 892.3481 and 1038.1058, corresponding to species having lost four and three PF_6^- counterions, that is $[M - 4PF_6]^{4+}$ and $[M - 3PF_6]^{3+}$, respectively.

^{1}H NMR Measurements. Next, we investigated the reversible acid−base-driven translocation movement of the DB24C8 macrocycles between the DBA and MTA stations in the system of rotaxane Fc−PBI, which was confirmed by ^{1}H NMR and 2D Roesy NMR spectroscopies, as discussed below. Upon the addition of 2.5 equiv of 1,8-diazabicyclo[5.4.0]undec-7-ene (DBU) into CD_3COCD_3 solution of Fc−PBI, the DBA moiety was deprotonated, which resulted in the migration of MTA recognition station into the DB24C8 ring and in the observation of obvious ^{1}H NMR spectral changes (Figure 1). As shown in Figure 1b, the peaks for the methylene protons H_{15} and H_{16} on the DBA recognition site were split and shifted upfield ($\Delta\delta$ = −0.54 and −0.63 ppm, respectively), which could be due to the dissociation effects of the deprotonation of the DBA centers and the mechanical moving of the DB24C8 rings.

On the other hand, the protons H_{25} and H_{26} on the MTA recognition station were also shifted with $\Delta\delta$ values of 0.23 and −0.47 ppm, respectively. Moreover, the peak of the phenyl protons H_{28} on the PBI was also shifted upfield with a $\Delta\delta$ value of −0.07 ppm. These indicated that the macrocycles DB24C8 were located on the MTA sites in both rotaxane arms upon the addition of excess DBU. Furthermore, 2D Roesy NMR spectra of DBU-added CD_3COCD_3 solution of rotaxane Fc−PBI also confirmed that the MTA sites migrated into the DB24C8 rings upon addition of DBU (ESI; Figure S1b, Supporting Information). Meanwhile, the generated dibenzylamine center was reprotonated by adding 5.0 equiv of CF_3COOH (TFA) that resulted in the recovery of the original ^{1}H NMR spectrum (Figure 1c), which suggested that the DBA stations were encircled completely by the macrocycles again. Using ^{1}H NMR and 2D Roesy NMR spectroscopies, we have proved the reversible translational motion of the molecular thread relative to the macrocycle in each rotaxane arm in CD_3COCD_3 solution.

Photophysical Properties and Molecular Dynamics Simulations of [1]Rotaxane Fc−PBI. The absorption spectrum of [1]rotaxane Fc−PBI in acetone (Figure 2a) shows three main absorption wavelength at λ_{max} = 440, 543, and 580 nm, which exhibit all the typical spectroscopic features of tetraphenoxy-substituted perylene bisimide chromophores.[58] UV−vis absorption and fluorescence spectral changes were observed in [1]rotaxane Fc−PBI in response to chemical stimuli. After adding 2.5 equiv of DBU to the acetone solution of Fc−PBI, the maximum UV−vis absorption wavelength had a red shift of about 7 nm. At the same time, compared with the original spectrum, the emission intensity of the PBI core at 612 nm decreased 86% upon the addition of 2.5 equiv of DBU (Figure 2b). These phenomena could be ascribed to a closer spatial distance between the ferrocene-functionalized DB24C8 rings and PBI fluorophore upon the addition of DBU. To further investigate these results, we carried out theoretical simulations of different states of the rotaxane Fc−PBI at 298 K in acetone for 10 ns. Starting from the optimized geometries, molecular dynamics simulations were conducted, employing the general Amber force field[59] in combination with the parameters for ferrocene developed by Lopes et al.[60] Snapshots for the rotaxane at two different states are shown in Figure 3. The average distance between the two Fe(II) centers and the PBI unit is 3.03 ± 0.51 nm in the original state 1; however, deprotonation of the DBA site leads to a closer spatial distance between the two Fe(II) centers and the PBI unit at state 2 (1.67 ± 0.27 nm; Table 1 and Figure S3c, Supporting Information). Thus, the distance-dependent photoinduced electron transfer (PET) process from the electron-rich Fc units to the electron-deficient PBI fluorophore became more efficient in the deprotonated state 2, resulting in fluorescence quenching. The UV−vis absorption and fluorescence spectra could also be recovered upon addition of 5.0 equiv of TFA, which can be observed visually, indicating that the UV−vis absorption and fluorescence spectra of this system can be reversibly adjusted using chemical stimuli (acid/base), even after repeated cycles (Figure S2, Supporting Information).

The conformational changes at different states obtained from molecular dynamics simulations indicate that the *bis*-branched [1]rotaxane system can perform dual-mode coupling motions in response to external stimuli. It can be seen in Figure 3 that the rotaxane in state 1 has its two crown ether macrocyles encircled at the protonated amine groups and features an

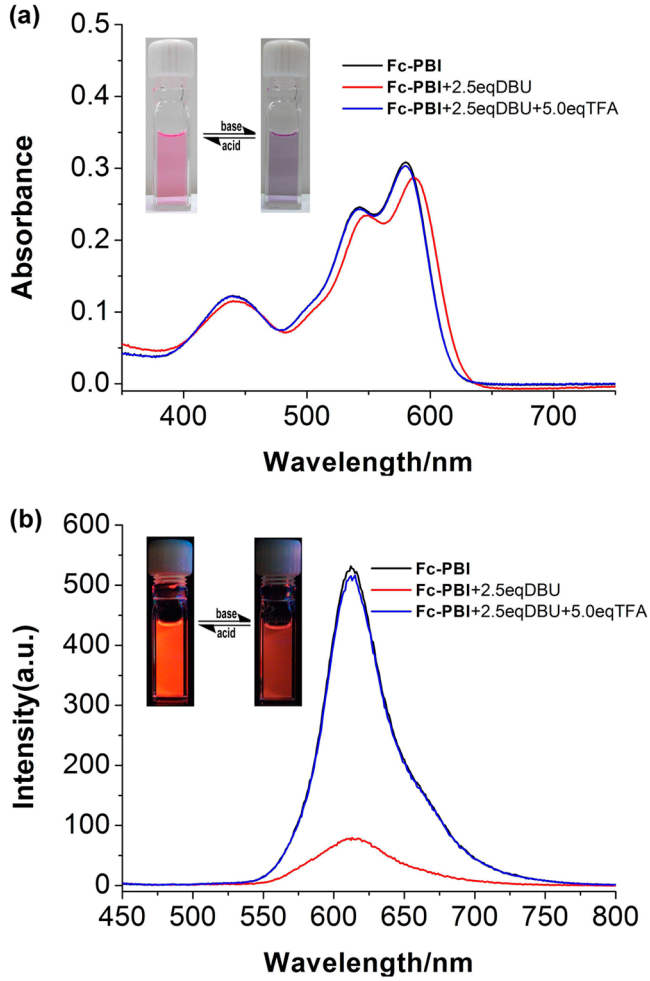

Figure 2. (a) UV−vis absorption spectral changes and (b) fluorescence spectral changes in acetone solution (1×10^{-5} M) of Fc−PBI, the mixture obtained after adding 2.5 equiv of DBU to the solution of Fc−PBI, and the mixture obtained after adding 5.0 equiv of TFA to the DBU-added solution of Fc−PBI. (Insets) Pictures of corresponding changes in UV−vis absorption and fluorescence. Excitation wavelength of all fluorescence spectra was 440 nm.

extended conformation, which could be attributed to the electrostatic repulsion between the MTA cations and the protonated amine groups. The average lengths of the extended conformation is about 6.11 ± 0.88 nm; however, at state 2 the two crown ether macrocyles encircle on the MTA stations, and the optimized structure corresponds to a contracted conformation (4.38 ± 0.54 nm), where the central perylene unit could form $\pi-\pi$ stack with the phenyl ring in one of the crown ether macrocyles. The percentage change in an average molecular length is about 28.3% between the two states, which is similar to the percentage change (~27%) in human muscle. Interestingly, the ferrocene terminal unit adopts different rotational conformations in two different states, as shown in Table 1 and Figure S3a (Supporting Information). We then monitored the C*−Cp−Cp−C* dihedral angle in the ferrocene unit, where C* and Cp denote the substitution position and the center of the two Cp rings of ferrocene moiety, respectively. In state 1, the two C*−Cp−Cp−C* dihedral angles of the ferrocene units are averaged as 105.5° and 26.8°, respectively, while in state 2, these two dihedral angles become −61.5° and −35.4°, respectively. The optimized

dx.doi.org/10.1021/am506283g | ACS Appl. Mater. Interfaces 2014, 6, 18921−18929

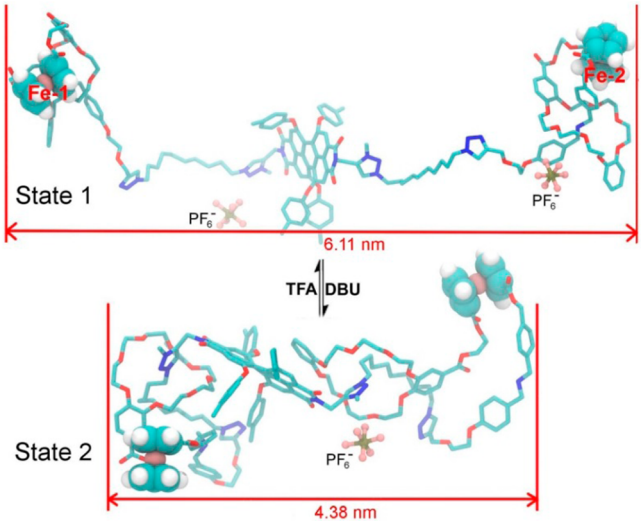

Figure 3. Schematic illustrations of the structures of the rotaxane Fc–PBI at the two states extracted from molecular dynamics trajectories. The optimized conformations at different states were obtained through molecular dynamics simulations employing the general Amber force field.

conformations at the two states indicate that the *bis*-branched system can perform reversible dual-mode coupling molecular motions: chemical stimuli can result in the relative movement of the ring and the molecular thread, thus inducing the extension-contraction movement of the system. This is accompanied by a simultaneous rotational movement of the two terminal ferrocene units, mimicking the function of a molecular machine with dual-mode movement type.

Tunable Molecular Aggregation of [1]Rotaxane Fc–PBI. In this system, PBI fluorescent dye was introduced not only as a fluorescent moiety to monitor the molecular motions, but also as an adjustable molecular aggregation unit, the aggregation of which can lead to either a red-shifted and narrowed or a blue-shifted and broadened absorption spectra in response to temperature,[61,62] solvent,[63,64] or concentration.[65] To gain further insight into the molecular aggregation properties of [1]rotaxane Fc–PBI, the solvent-dependent UV–vis and fluorescence emission spectra were studied. As shown in Figure 4a, the UV–vis absorption maximum (λ_{max}) gradually decreased and then red-shifted with the increasing proportion of methylcyclohexane (MCH, low polarity) in acetone (high polarity) solution of rotaxane Fc–PBI under the same concentration (1×10^{-5} M). This is also accompanied by a decrease in fluorescence (Figure 4b). These results can be ascribed to the degree of π–π stacking aggregation of the PBI in rotaxane Fc–PBI. In other words, upon the addition of MCH to the acetone solution of Fc–PBI, the polarity of the mixed solution is slowly reduced, and the degree of aggregation of the PBI in rotaxane Fc–PBI is enhanced, which results in the

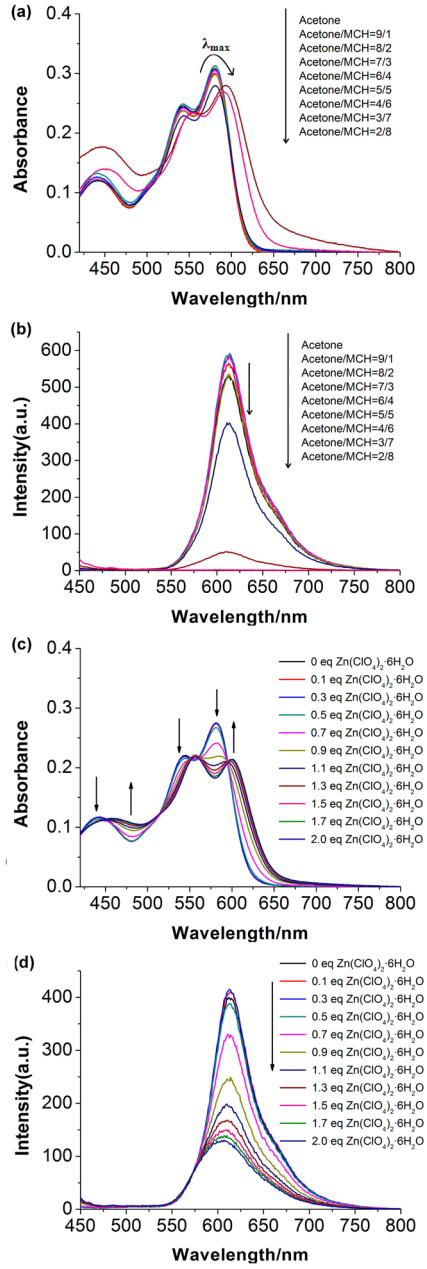

Figure 4. (a) UV–vis spectral changes and (b) corresponding fluorescence emission spectral changes of [1]rotaxane Fc–PBI (1×10^{-5} M) in different ratios of acetone and methylcyclohexane (MCH; v/v), (c) UV–vis spectral changes and (d) corresponding fluorescence emission spectral changes of [1]rotaxane Fc–PBI (1×10^{-5} M) during a titration of $Zn(ClO_4)_2 \cdot 6H_2O$ in acetone/MCH solvent mixtures of 1:1 (v/v); corresponding fluorescence emission spectral changes with λ_{ex} fixed at 440 nm; arrows indicate the changes in the spectra with increasing the concentration of $Zn(ClO_4)_2 \cdot 6H_2O$ (0–2.0 equiv).

Table 1. Average Length of the Rotaxane, Fe–Fe Distance of the Dumbbell, Distance between the Fe(II) Center and the PBI Unit, and the C*–Cp–Cp–C* Dihedral Angle of Ferrocene[a]

			$d_{Fe\text{-}PBI}$ (nm)		$\varphi_{C^*\text{–}Cp\text{–}Cp\text{–}C^*}$ (deg)	
	average length (nm)	$d_{Fe\text{–}Fe}$ (nm)	Fe-1	Fe-2	Fe-1	Fe-2
state 1	6.11 ± 0.88	4.19 ± 0.49	3.11 ± 0.37	2.95 ± 0.64	105.5 ± 53.3	26.8 ± 17.8
state 2	4.38 ± 0.54	3.17 ± 0.38	1.78 ± 0.31	1.55 ± 0.23	−61.5 ± 44.9	−35.4 ± 37.2

[a]Each quantity is listed as an average over the last 5 ns of simulation trajectory together with its standard deviation.

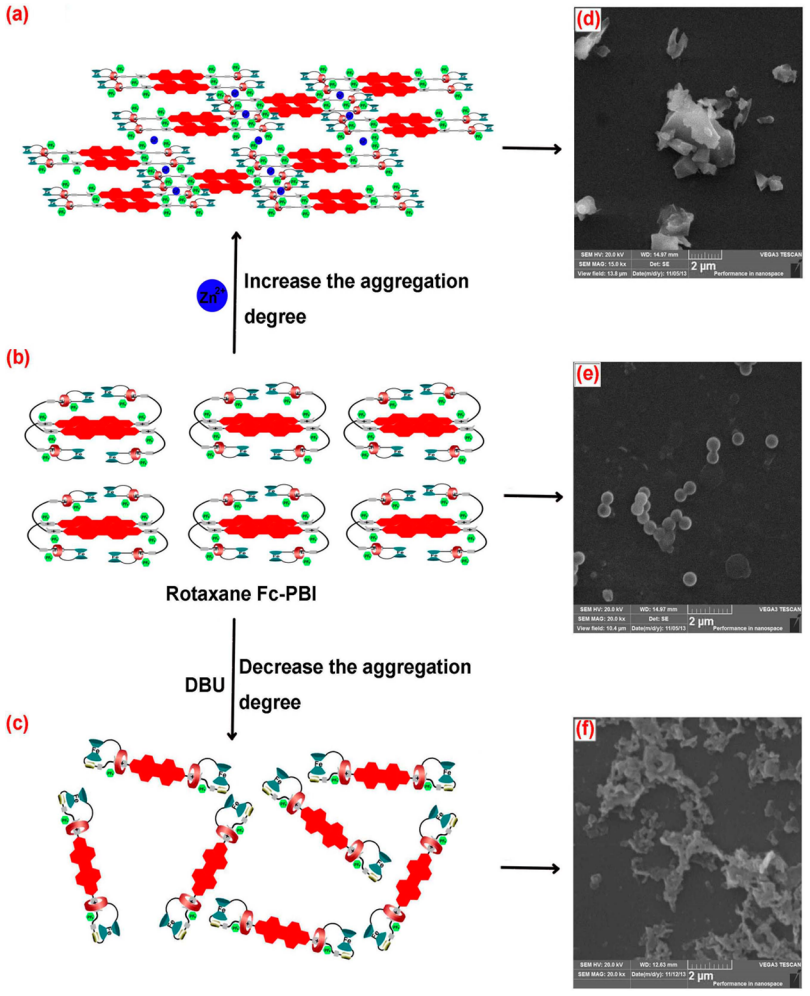

Figure 5. Schematic representation of the formation of [1]rotaxane Fc−PBI nanostructures in different conditions: (a) obtained after the addition of 2.0 equiv of Zn^{2+} to the solution of Fc−PBI (1×10^{-5} M) in acetone/MCH solvent mixtures of 1:1 (v/v); (b) rotaxane Fc−PBI; and (c) obtained after the addition of 2.5 equiv of DBU to the solution of Fc−PBI. SEM images of (d) the structures obtained after the addition of 2.0 equiv of Zn^{2+} to the solution of Fc−PBI (1×10^{-5} M) in acetone/MCH solvent mixtures of 1:1 (v/v); (e) rotaxane Fc−PBI; and (f) the structure obtained after the addition of 2.5 equiv of DBU to the solution of Fc−PBI.

red-shifted UV−vis absorption and quenched fluorescence. Similar results are also observed for the mixed solution of dichloromethane/MCH and 1,2-dichloroethane/MCH of rotaxane Fc−PBI (Figure S4, Supporting Information), which indicates that the system is in an aggregated state in the mixed solvents. Furthermore, the coordination between the 1,2,3-triazole units of the Fc−PBI and transition metal Zn^{2+} was proved by the changes of ^{1}H NMR spectra of Fc−PBI upon different concentrations of $Zn(ClO_4)_2{\cdot}6H_2O$ (0−2.0 equiv; Figure S5, Supporting Information), and their effects were investigated by undertaking measurements of UV−vis absorption spectra and fluorescence emission spectra. As shown in Figure 4, upon increasing the concentration of $Zn(ClO_4)_2{\cdot}6H_2O$ (0−2.0 equiv) in acetone/MCH solvent mixtures of 1:1 (v/v) of Fc−PBI, the UV−vis spectra (Figure 4c) exhibit a clear bathochromical shift accompanied by a decreased intensity. The maximum of the absorption band was red-shifted 19 nm to λ_{max} = 601 nm with two well-defined isosbestic points at 511 and 596 nm. Meanwhile, fluorescence intensity (Figure 4d) also decreased. These phenomena can also be attributed to the fact that the PBI units have a higher aggregation degree upon the addition of Zn^{2+}, due to the coordination with the 1,2,3-triazoles of the Fc−PBI. However, it should be noted that we also investigated the aggregation behaviors of DBU-added Fc−PBI upon the addition of Zn^{2+} (Figure S7, Supporting Information). As a result, there is a stronger aggregation degree under the higher concentration of Zn^{2+} (>1.1 equiv) in the DBU-added Fc−PBI system.

Aggregation Morphologies and Proposed Mechanisms of [1]Rotaxane Fc−PBI. The aggregated nanostructural morphologies of [1]rotaxane Fc−PBI in different conditions were examined by scanning electron microscopy (SEM; Figure 5) and their possible aggregation mechanisms from molecular structures to the morphologies of the nanostructures were also proposed. In the acetone/MCH solvent mixtures of 1:1 (v/v) (Figure 5b), the intermolecular $\pi-\pi$ interactions drag two or more PBI units close to each other owing to the low polarity of the solvent, forming the actual building blocks for the generated nanospheres (d = ∼ 200 nm; Figure 5e). More interestingly, upon the addition of $Zn(ClO_4)_2{\cdot}6H_2O$ and chelation of Zn^{2+} ions by the neutral 1,2,3-triazoles unit of the rotaxane, a more compact self-assembly is formed because many molecular aggregations formed without Zn^{2+} can move close to each other due to the Zn^{2+}-assisted self-assembly of the rotaxane. Furthermore, because each rotaxane has two neutral 1,2,3-triazole chelation

sites, there are also possibilities of forming cross-linked structures among the Zn^{2+} ions and rotaxanes,[66] which can further strengthen the aggregation (Figure 5a). Therefore, the SEM image shows that some amorphous crystals of bigger size appeared after adding 2.0 equiv of $Zn(ClO_4)_2 \cdot 6H_2O$ to the solution of Fc−PBI (Figure 5d). Differently, after addition of 2.5 equiv of DBU to the solution of Fc−PBI, the amine groups become unprotonated and the crown ether macrocyles encircle on the MTA stations, which not only decreases the solvent-accessible surface area of the rotaxane as reflected by a small length of the molecule but also hampers the $\pi-\pi$ interactions between adjacent PBI units (Figure 5c), leading to the formation of the amorphous morphology (Figure 5f), which is also proved by the results of the solvent-dependent UV−vis and fluorescence emission spectra of DBU-added [1]rotaxane Fc−PBI (Figure S6, Supporting Information). Furthermore, these results are consistent with the simulation of the self-assembly of rotaxane Fc−PBI dimers under the different conditions obtained in acetone/MCH (1:1) solution (Figure S10, Supporting Information). In short, the aggregation behavior of rotaxane Fc−PBI can be affected by two factors: the addition of Zn^{2+} can increase the aggregation degree of the system, while the addition of DBU hinders aggregation because of the shuttling motion of the macrocycle.

CONCLUSIONS

Inspired by naturally occurring biological motors and the possibility of controlling molecular motions in molecular machine systems, we have, in this work, prepared and studied a multifunctional *bis*-branched [1]rotaxane that contains a perylene bisimide unit as a core and two [1]rotaxane arms with terminal ferrocene functional units. The system undergoes relative mechanical movements of its ring and thread in response to external acid−base stimuli, which can induce the extension and contraction movements of the whole system, accompanied by the rotational movement of the ferrocene units. These results pave the way to achieve precise control of integrated and coupled nanomechanical motions at a single-molecule level. Moreover, the control of the aggregation degree of perylene bisimide unit can be realized through the moving of macrocycles by the addition of DBU and the coordination of the 1,2,3-triazole chelation site with Zn^{2+} cations, respectively. The addition of DBU can decrease the aggregation degree of the system, while the addition of Zn^{2+} cations enhances it. It should be noted that the introduction of the perylene bisimide unit not only enables the system with fluorescence encoding but also facilitates a controllable tunability of molecular aggregation with diverse nanostructural morphologies. This provides more insight of possible applications of switchable mechanically interlocked molecules, for instance, in the areas of supramolecular materials science.

ASSOCIATED CONTENT

Supporting Information

Detailed experimental procedures and molecular dynamics simulations of target [1]rotaxane Fc−PBI and spectral data for all new compounds. This material is available free of charge via the Internet at http://pubs.acs.org.

AUTHOR INFORMATION

Corresponding Author

*E-mail: dahui_qu@ecust.edu.cn. Fax: +86-21 64250940.

Notes

The authors declare no competing financial interest.

ACKNOWLEDGMENTS

We thank the NSFC/China (21272073, 21190033) and the National Basic Research 973 Program (2011CB808400), the Fok Ying Tong Education Foundation (121069), the Fundamental Research Funds for the Central Universities, the Innovation Program of Shanghai Municipal Education Commission, and the Science Fund for Creative Research Groups (No. 21421004) for financial support.

REFERENCES

(1) Kinbara, K.; Aida, T. Toward Intelligent Molecular Machines: Directed Motions of Biological and Artificial Molecules and Assemblies. *Chem. Rev.* **2005**, *105*, 1377−1400.
(2) Saha, S.; Stoddart, J. F. Photo-Driven Molecular Devices. *Chem. Soc. Rev.* **2007**, *36*, 77.
(3) Coskun, A.; Friedman, D. C.; Li, H.; Patel, K.; Khatib, H. A.; Stoddart, J. F. A Light-Gated STOP−GO Molecular Shuttle. *J. Am. Chem. Soc.* **2009**, *131*, 2493−2495.
(4) Blanco, V.; Leigh, D. A.; Marcos, V.; Morales-Serna, J. A.; Nussbaumer, A. L. A Switchable [2]Rotaxane Asymmetric Organocatalyst That Utilizes an Acyclic Chiral Secondary Amine. *J. Am. Chem. Soc.* **2014**, *136*, 4905−4908.
(5) Sauvage, J.-P.; Gaspard, P.; Balzani, V.; Credi, A.; Venturi, A. *Molecular Machines Based on Rotaxanes and Catenanes*; Wiley-VCH: Weinheim, Germany, 2010.
(6) Dasgupta, S.; Wu, J.-S. Formation of [2]Rotaxanes by Encircling [20], [21], and [22] Crown Ethers onto the Dibenzylammonium Dumbbell. *Chem. Sci.* **2012**, *3*, 425−432.
(7) Stadler, A.-M.; Lehn, J.-M. Coupled Nanomechanical Motions: Metal-Ion-Effected, pH-Modulated, Simultaneous Extension/Contraction Motions of Double-Domain Helical/Linear Molecular Strands. *J. Am. Chem. Soc.* **2014**, *136*, 3400−3409.
(8) Yang, W.-L.; Li, Y.-J.; Liu, H.-B.; Chi, L.-F.; Li, Y.-L. Design and Assembly of Rotaxane-Based Molecular Switches and Machines. *Small* **2012**, *8*, 504−516.
(9) Mandl, C. P.; König, B. Chemistry in Motion—Unidirectional Rotating Molecular Motors. *Angew. Chem., Int. Ed.* **2004**, *43*, 1622−1624.
(10) Pollard, M. M.; Lubomska, M.; Rudolf, P.; Feringa, B. L. Controlled Rotary Motion in a Monolayer of Molecular Motors. *Angew. Chem., Int. Ed.* **2007**, *46*, 1278−1280.
(11) Mateo-Alonso, A.; Ehli, C.; Guldi, D. M.; Prato, M. Charge Transfer Reactions along a Supramolecular Redox Gradient. *J. Am. Chem. Soc.* **2008**, *130*, 14938−14939.
(12) Meng, Z.; Xiang, J.-F.; Chen, C.-F. Tristable [n]Rotaxanes: From Molecular Shuttle to Molecular Cable Car. *Chem. Sci.* **2014**, *5*, 1520−1525.
(13) Zhang, H.; Hu, J.; Qu, D.-H. Dual-Mode Control of PET Process in a Ferrocene-Functionalized [2]Rotaxane with High-Contrast Fluorescence Output. *Org. Lett.* **2012**, *14*, 2334−2337.
(14) Zhu, L.-L.; Yan, H.; Wang, X.-J.; Zhao, Y.-L. Light-Controllable Cucurbit[7]uril-based Molecular Shuttle. *J. Org. Chem.* **2012**, *77*, 10168−10175.
(15) Zhang, J.-N.; Li, H.; Zhou, W.; Yu, S.-L.; Qu, D.-H.; Tian, H. Fluorescence Modulation in Tribranched Switchable [4]Rotaxanes. *Chem.−Eur. J.* **2013**, *19*, 17192−17200.
(16) Muraoka, T.; Kinbara, K.; Kobayashi, Y.; Aida, T. Light-Driven Open-Close Motion of Chiral Molecular Scissors. *J. Am. Chem. Soc.* **2003**, *125*, 5612−5613.
(17) Muraoka, T.; Kinbara, K.; Aida, T. Mechanical Twisting of a Guest by a Photoresponsive Host. *Nature* **2006**, *440*, 512−515.
(18) Kai, H.; Nara, S.; Kinbara, K.; Aida, T. Toward Long-Distance Mechanical Communication: Studies on a Ternary Complex Interconnected by a Bridging Rotary Module. *J. Am. Chem. Soc.* **2008**, *130*, 6725−6727.

(19) Chuang, C.-J.; Li, W.-S.; Lai, C.-C.; Liu, Y.-H.; Peng, S.-M.; Chao, I.; Chiu, S.-H. A Molecular Cage-Based [2]Rotaxane That Behaves as a Molecular Muscle. *Org. Lett.* **2009**, *11*, 385−388.
(20) Ma, X.; Tian, H. Bright Functional Rotaxanes. *Chem. Soc. Rev.* **2010**, *39*, 70−80.
(21) Du, G.-Y.; Moulin, E.; Jouault, N.; Buhler, E.; Giuseppone, N. Muscle-Like Supramolecular Polymers: Integrated Motion from Thousands of Molecular Machines. *Angew. Chem., Int. Ed.* **2012**, *51*, 12504−12508.
(22) Bruns, C. J.; Stoddart, J. F. Supramolecular Polymers: Molecular Machines Muscle Up. *Nat. Nanotechnol.* **2013**, *8*, 9−10.
(23) Badjic, J. D.; Balzani, V.; Credi, A.; Silvi, S.; Stoddart, J. F. A Molecular Elevator. *Science* **2004**, *303*, 1845−1849.
(24) Badjic, J. D.; Ronconi, C. M.; Stoddart, J. F.; Balzani, V.; Silvi, S.; Credi, A. Operating Molecular Elevators. *J. Am. Chem. Soc.* **2006**, *128*, 1489−1499.
(25) Zhang, Z.-J.; Han, M.; Zhang, H.-Y.; Liu, Y. A Double-Leg Donor-Acceptor Molecular Elevator: New Insight into Controlling the Distance of Two Platforms. *Org. Lett.* **2013**, *15*, 1698−1701.
(26) Delius, M. V.; Geertsema, E. M.; Leigh, D. A. A Synthetic Small Molecule that Can Walk Down A Track. *Nat. Chem.* **2009**, *2*, 96−101.
(27) Delius, M. V.; Leigh, D. A. Walking Molecules. *Chem. Soc. Rev.* **2011**, *40*, 3656−3676.
(28) Lewandowski, B.; Bo, G. D.; Ward, J. W.; Papmeyer, M.; Kuschel, S.; Aldegunde, M. J.; Gramlich, P. M. E.; Heckmann, D.; Goldup, S. M.; D'Souza, D. M.; Fernandes, A. E.; Leigh, D. A. Sequence-Specific Peptide Synthesis by an Artificial Small-Molecule Machine. *Science* **2013**, *339*, 189−193.
(29) Qu, D.-H.; Tian, H. Synthetic Small-Molecule Walkers at Work. *Chem. Sci.* **2013**, *4*, 3031−3035.
(30) Beves, J. E.; Blanco, V.; Blight, B. A.; Carrillo, R.; D'Souza, D. M.; Howgego, D.; Leigh, D. A.; Slawin, A. M. Z.; Symes, M. D. Toward Metal Complexes That Can Directionally Walk Along Tracks: Controlled Stepping of a Molecular Biped with a Palladium(II) Foot. *J. Am. Chem. Soc.* **2014**, *136*, 2094−2100.
(31) Flood, A. H.; Stoddart, J. F.; Steuerman, D. W.; Heath, J. R. Whence Molecular Electronics? *Science* **2004**, *306*, 2055−2056.
(32) Hiratani, K.; Kaneyama, M.; Nagawa, Y.; Koyama, E.; Kanesato, M. Synthesis of [1]Rotaxane via Covalent Bond Formation and Its Unique Fluorescent Response by Energy Transfer in the Presence of Lithium Ion. *J. Am. Chem. Soc.* **2004**, *126*, 13568−13569.
(33) Li, H.; Zhang, J.-N.; Zhou, W.; Zhang, H.; Zhang, Q.; Qu, D.-H.; Tian, H. Dual-Mode Operation of a Bistable [1]Rotaxane with a Fluorescence Signal. *Org. Lett.* **2013**, *15*, 3070−3073.
(34) Li, H.; Zhang, H.; Zhang, Q.; Zhang, Q.-W.; Qu, D.-H. A Switchable Ferrocene-Based [1]Rotaxane with an Electrochemical Signal Output. *Org. Lett.* **2012**, *14*, 5900−5903.
(35) Motta, S. D.; Avellini, T.; Silvi, S.; Venturi, M.; Ma, X.; Tian, H.; Credi, A.; Negri, F. Photophysical Properties and Conformational Effects on the Circular Dichroism of an Azobenzene-Cyclodextrin [1]Rotaxane and Its Molecular Components. *Chem.−Eur. J.* **2013**, *19*, 3131−3138.
(36) Bordoli, R. J.; Goldup, S. M. An Efficient Approach to Mechanically Planar Chiral Rotaxanes. *J. Am. Chem. Soc.* **2014**, *136*, 4817−4820.
(37) Lehn, J.-M. *Supramolecular Chemistry: Concepts and Perspectives*; Wiley-VCH: Weinheim, Germany, 1995.
(38) Grimsdale, A. C.; Müllen, K. The Chemistry of Organic Nanomaterials. *Angew. Chem., Int. Ed.* **2005**, *44*, 5592−5629.
(39) Zhou, W.-D.; Xu, J.-L.; Zheng, H.-Y.; Yin, X.-D.; Zuo, Z.-C.; Liu, H.-B.; Li, Y.-L. Distinct Nanostructures from a Molecular Shuttle: Effects of Shuttling Movement on Nanostructural Morphologies. *Adv. Funct. Mater.* **2009**, *19*, 141−149.
(40) Jiang, Y.; Guo, J.-B.; Chen, C.-F. A New [3]Rotaxane Molecular Machine Based on a Dibenzylammonium Ion and a Triazolium Station. *Org. Lett.* **2010**, *12*, 4248−4251.
(41) Clavel, C.; Romuald, C.; Brabet, E.; Coutrot, F. A pH-Sensitive Lasso-Based Rotaxane Molecular Switch. *Chem.−Eur. J.* **2013**, *19*, 2982−2989.
(42) Zhou, W.; Guo, Y.-J.; Qu, D.-H. Photodriven Clamlike Motion in a [3]Rotaxane with Two [2]Rotaxane Arms Bridged by an Overcrowded Alkene Switch. *J. Org. Chem.* **2013**, *78*, 590−596.
(43) Coutrot, F.; Romuald, C.; Busseron, E. A New pH-Switchable Dimannosyl[c2]Daisy Chain Molecular Machine. *Org. Lett.* **2008**, *10*, 3741−3744.
(44) Hänni, K. D.; Leigh, D. A. The Application of CuAAC 'Click' Chemistry to Catenane and Rotaxane Synthesis. *Chem. Soc. Rev.* **2010**, *39*, 1240−1251.
(45) Zhang, H.; Zhou, B.; Li, H.; Qu, D.-H.; Tian, H. A Ferrocene-Functionalized [2]Rotaxane with Two Fluorophores as Stoppers. *J. Org. Chem.* **2013**, *78*, 2091−2098.
(46) Mateo-Alonso, A.; Ehli, C.; Guldi, D. M.; Prato, M. A Three-Level Luminescent Response in a Pyrene/Ferrocene Rotaxane. *Org. Lett.* **2013**, *15*, 84−87.
(47) Zhang, D.; Zhang, Q.; Su, J.-H.; Tian, H. A Dual-Ion-Switched Molecular Brake Based on Ferrocene. *Chem. Commun.* **2009**, 1700−1702.
(48) Iordache, A.; Oltean, M.; Milet, A.; Thomas, F.; Baptiste, B.; Saint-Aman, E.; Bucher, C. Redox Control of Rotary Motions in Ferrocene-Based Elemental Ball Bearings. *J. Am. Chem. Soc.* **2012**, *134*, 2653−2671.
(49) Seybold, G.; Wagenblast, G. New Perylene and Violanthrone Dyestuffs for Fluorescent Collectors. *Dyes Pigm.* **1989**, *11*, 303−317.
(50) Gvishi, R.; Reisfeld, R.; Burshtein, Z. Spectroscopy and Laser Action of the "Red Perylimide Dye" in Various Solvents. *Chem. Phys. Lett.* **1993**, *213*, 338−344.
(51) Li, Y.-J.; Wang, N.; Gan, H.-Y.; Liu, H.-B.; Li, H.; Li, Y.-L.; He, X.-R.; Huang, C.-S.; Cui, S.; Wang, S.; Zhu, D.-B. Synthesis and Characterization of 3,5-Bis(2-hydroxyphenyl)-1,2,4-triazole Functionalized Tetraaryloxy Perylene Bisimide and Metal-Directed Self-Assembly. *J. Org. Chem.* **2005**, *70*, 9686−9692.
(52) Würthner, F.; Kaiser, T. E.; Saha-Möller, C. R. J-Aggregates: From Serendipitous Discovery to Supramolecular Engineering of Functional Dye Materials. *Angew. Chem., Int. Ed.* **2011**, *50*, 3376−3410.
(53) Takashima, Y.; Fukui, Y.; Otsubo, M.; Hamada, N.; Yamaguchi, H.; Yamamoto, H.; Harada, A. Emission Properties of Cyclodextrin Dimers Linked with Perylene Diimide-Effect of Cyclodextrin Tumbling. *Polym. J.* **2012**, *44*, 278−285.
(54) Shao, C.-Z.; Stolte, M.; Würthner, F. Quadruple π Stack of Two Perylene Bisimide Tweezers: A Bimolecular Complex with Kinetic Stability. *Angew. Chem., Int. Ed.* **2013**, *52*, 7482−7486.
(55) El-Batal, H.; Guo, K.; Li, X.-P.; Wesdemiotis, C.; Moorefield, C. N.; Newkome, G. R. Perylene-Based Bis-, Tetrakis-, and Hexakis-(terpyridine) Ligands and Their Ruthenium (II)-Bis(terpyridine) Complexes: Synthesis and Photophysical Properties. *Eur. J. Org. Chem.* **2013**, *2013*, 3640−3644.
(56) Cho, J.; Pradhan, T.; Kim, J. S.; Kim, S. Bimodal Calix[2]-triazole[2]arene Fluorescent Ionophore. *Org. Lett.* **2013**, *15*, 4058−4061.
(57) Winn, J.; Pinczewska, A.; Goldup, S. M. Synthesis of a Rotaxane CuI Triazolide under Aqueous Conditions. *J. Am. Chem. Soc.* **2013**, *135*, 13318−13321.
(58) Würthner, F. Bay-Substituted Perylene Bisimides: Twisted Fluorophores for Supramolecular Chemistry. *Pure Appl. Chem.* **2006**, *78*, 2341−2349.
(59) Wang, J.; Wolf, R. M.; Caldwell, J. W.; Kollman, P. A.; Case, D. A. Development and Testing of a General Amber Force Field. *J. Comput. Chem.* **2004**, *25*, 1157−1174.
(60) Lopes, J. N. C.; do Couto, P. C.; da Piedade, M. E. M. An All-Atom Force Field for Metallocenes. *J. Phys. Chem. A* **2006**, *110*, 13850−13856.
(61) Kaiser, T. E.; Wang, H.; Stepanenko, V.; Würthner, F. Supramolecular Construction of Fluorescent J-Aggregates Based on Hydrogen-Bonded Perylene Dyes. *Angew. Chem., Int. Ed.* **2007**, *46*, 5541−5544.
(62) Chen, Z.-J.; Stepanenko, V.; Dehm, V.; Prins, P.; Siebbeles, L. D. A.; Seibt, J.; Marquetand, P.; Engel, V.; Würthner, F. Photo-

luminescence and Conductivity of Self-Assembled $\pi-\pi$ Stacks of Perylene Bisimide Dyes. *Chem.—Eur. J.* **2007**, *13*, 436—449.
(63) Grzelczak, M.; Kulisic, N.; Prato, M.; Mateo-Alonso, A. Multimode Assembly of Phenanthroline Nanowires Decorated with Gold Nanoparticles. *Chem. Commun.* **2010**, *46*, 9122—9124.
(64) Dehm, V.; Büuchner, M.; Seibt, J.; Engel, V.; Würthner, F. Foldamer with a Spiral Perylene Bisimide Staircase Aggregate Structure. *Chem. Sci.* **2011**, *2*, 2094—2100.
(65) Kaiser, T. E.; Stepanenko, V.; Würthner, F. Fluorescent J-Aggregates of Core-Substituted Perylene Bisimides: Studies on Structure-Property Relationship, Nucleation-Elongation Mechanism, and Sergeants-and-Soldiers Principle. *J. Am. Chem. Soc.* **2009**, *131*, 6719—6732.
(66) Wang, F.; Zhang, J.-Q.; Ding, X.; Dong, S.-Y.; Liu, M.; Zheng, B.; Li, S.-J.; Wu, L.; Yu, Y.-H.; Gibson, H. W.; Huang, F.-H. Metal Coordination Mediated Reversible Conversion between Linear and Cross-Linked Supramolecular Polymers. *Angew. Chem., Int. Ed.* **2010**, *49*, 1090—1094.